STRUCTURE AND INFRASTRUCTURE ENGINEERING
2021, AHEAD-OF-PRINT, 1-17
https://doi.org/10.1080/15732479.2021.1924796

Experimental investigation of the bearing capacity of deformed segmental tunnel linings strengthened by a special composite structure

Xian Liu[a,b], Zijie Jiang[a], and Herbert A. Mang[a,c]

[a] College of Civil Engineering, Tongji University, Shanghai, China [b] Key Laboratory of Performance Evolution and Control for Engineering Structures, Ministry of Education, Tongji University, Shanghai, China [c] Institute for Mechanics of Materials and Structures, Vienna University of Technology, Vienna, Austria

ABSTRACT

Steel plate – concrete composite structure (SPCCS) was recently proposed to strengthen shield tunnels. The steel plate serves as the strengthening material. A combination of connectors and steel-fiber reinforced concrete is employed to establish the bond between the strengthening material and the tunnel lining. A full-scale test was conducted to investigate the mechanical behavior and the bearing capacity of the structure. A comparison of the SPCCS strengthening technique with the epoxy-bonded steel plate (EBSP) strengthening technique was conducted, concerning the distribution of the strain of the steel plate, the joint opening, the bolt strain, slippage, the stripping value, the failure mechanism, and the overall strengthening benefits. The results are shown as follows: for the shield lining, strengthened by the SPCCS technique, the effectiveness of the bond increases, which renders acting of the individual structural components in combination with the tunnel lining more efficient, resulting in the full use of the components of the strengthening device. The failure mode of the strengthened structure is characterized by a high degree of ductility. Compared with EBSP strengthening, the SPCCS strengthening technique results in a reduction of the amount of steel, but in an increase of the bearing capacity and the ductility.

ARTICLE HISTORY
Received 21 September 2020
Revised 27 January 2021
Accepted 2 February 2021

KEYWORDS
Bearing capacity, composite structures, ductility, full-scale tests, shield tunnels, strengthening techniques

CONTACT Zijie Jiang jzj055880@tongji.edu.cn Key Laboratory of Performance Evolution and Control for Engineering Structures, Ministry of Education, Tongji University, Shanghai, China

1. Introduction

The development of underground metro systems can relieve pressure on urban transportation, which helps to reduce problems in consequence of population concentrations in metropoles. The shield tunneling method is environmentally friendly and mechanically effective. However, several structural problems may occur, such as e.g. cracking and spalling of concrete and leakage of water (Yuan, Jiang, & Liu, 2013). Partially, these problems are the consequence of faulty design, construction mistakes, or unexpected changes of the loading conditions. Apart from that, the discontinuities of the structure, in the form of the segmental joints connecting neighboring segments, are the main reason of the sensitivity of the structure with respect to the lateral load. Chang, Sun, Duann, and Hwang (2001) reported that the overburden of the vertical load and unloading of the horizontal load can significantly reduce the safety and the durability of segmental tunnel linings. As a remedy, strengthening is required in order to increase the resistance of the tunnel lining when the structure is suffering from the above-mentioned problems.

However, for metro tunnels in operation, strengthening of the structure can only be carried out at night. Moreover, the space, available for strengthening, is limited. Furthermore, restrictions on time and space render the design and the construction of segmental tunnel linings difficult.

Different techniques of strengthening tunnel linings are discussed in the literature. Kiriyama, Kakizaki, Takabayashi, Hirosawa, and Imafuku (2005) introduced a tunnel reinforcement technique using steel panels. Liu, Jiang, Yuan, and Mang (2018a) conducted full scale tests, employing a strengthening technique based on EBSP. Strengthening by means of fiber-reinforced polymer (FRP) (Liu, Zhang, Zhang, & Jiang, 2016) or by epoxy-bonded filament wound profiles (EBFWP) (Liu et al., 2018a; Liu, Jiang, & Zhang, 2017) was also investigated experimentally. In the EBSP strengthening technique the self-weight of the steel plate is so high that hoisting machines are needed for construction. The transportation of the hoisting machines to and out of the construction site takes much time, which makes this strengthening technique inefficient.

The FRP strengthening technique is convenient, and it can increase the bearing capacity significantly. However, the increase of the structural stiffness is much lower than the one obtained by the EBSP strengthening technique (Liu, Zhang, et al., 2016). The reason for this is that the thickness of the FRP is 0.2 mm, while the one of the steel plate is 20 mm. Hence, the moment of inertia of the cross-section strengthened by FRP is much smaller than the one strengthened by EBSP. The EBFWP strengthening technique reduces the self-weight of the strengthening material, which enables rapid construction (Liu, Jiang, et al., 2017). Moreover, the bearing capacity of the structure and its stiffness are increased significantly. However, failure in the framework of this strengthening technique is initiated by failure of the bond between the concrete segment and the strengthening material, rather than by failure of the materials.

Steel plate – concrete composite structures were thoroughly investigated and used (Narayanan, 1988) because of their good mechanical properties. Different types of composite structures (Sohel, Liew, Yan, Zhang, & Chia, 2012) and different shear connectors (Kozma, Odenbreit, Braun, Veljkovic, & Nijgh, 2019) between the steel plate and the concrete were also widely investigated. The effect of creep and shrinkage of the concrete on the composite beams were discussed in literatures. It is shown that the creep of concrete has unneglectable influence on the deformation of concrete beams in a long term (Liu, Erkmen, & Bradford, 2012; Wu, Gao, Feng, & Luo, 2016). Besides, the shrinkage of concrete in composite structure is restrained by studs and steel plates (Hua et al., 2020). These research works provide the basis for the proposal of a strengthening technique, using steel plate – concrete composite structures (SPCCS). For the first time, it was proposed by Nie, Wang, and Cai (2011). The load-carrying mechanism was investigated by means of a parametric analysis of RC beams.

An application of this strengthening technique is illustrated in Figure 1(a). Construction details of this technique are shown in Figure 1(b). The steel plate serves as the strengthening device. The steel bars, embedded in the RC beam, and the studs, welded to the surface of the steel plate, represent the shear connectors. The gap between the steel plate and the RC beam is filled with concrete (referred to as *new* concrete), which renders interaction of both constituents possible. A steel bar net is deployed into the gap before grouting of the concrete in order to increase the crack resistance of the new concrete. Shrinkage of the new concrete was neglected because of the restraint by the studs and steel plate. Furthermore, the influence of creep of the new concrete was also not considered in the research carried out by Nie et al. (2011). It is because that before the new concrete reached the 28-day-age strength, the concrete was not subjected to external loading. During the test, the beams strengthened by SPCCS technique, were loaded to the failure state in several hours. The effect of creep was not significant. These provide reference to the present research.

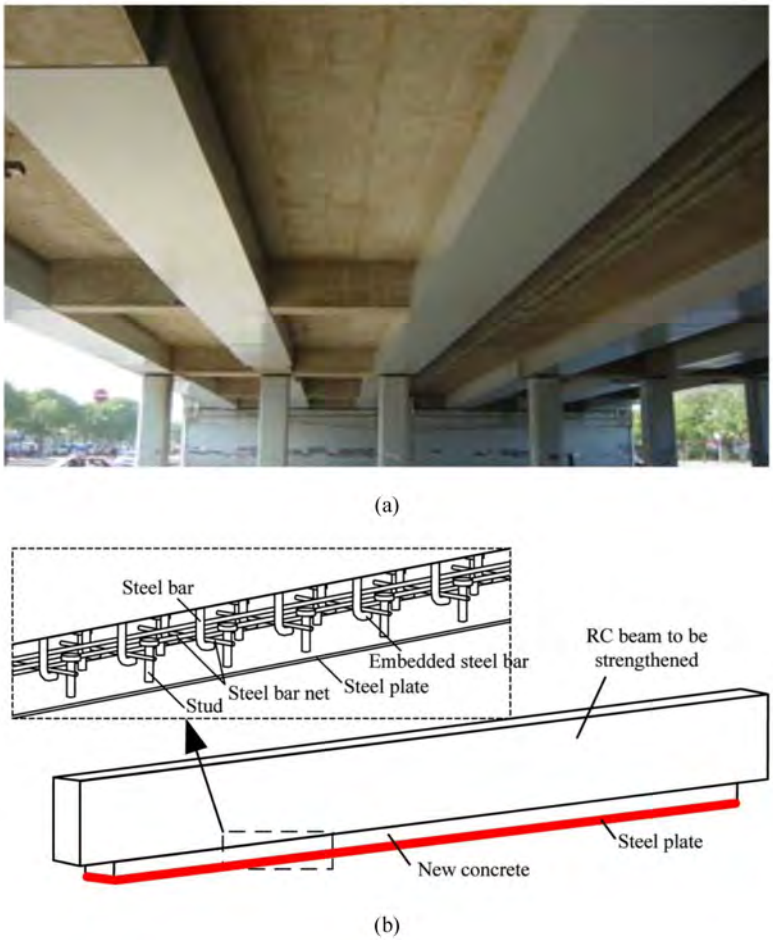

Figure 1. (a) Application of the SPCCS strengthening technique; (b) Construction details (Nie et al., 2011).

Since, as mentioned before, the construction space in shield tunnels is limited, the deployment of the steel bar net is a difficult task. On the other hand, previous research (Nie et al., 2011) only focused on the mechanical behavior of straight RC beams. It has shown that the SPCCS strengthening technique can improve the mechanical performance of these structural elements. In all of these investigations the shear resistance of the bond between the steel plate and the old concrete is calculated and designed. However, the tensile resistance in the direction normal to the bond only satisfies the detailing requirements. The situation in metro tunnels is different. The cross-sections of most segmental tunnel linings are circular. Thus, the segments represent curved beams. The force in the direction normal to the bond (radial force) is significant. The traditional SPCCS strengthening technique is unable to provide sufficient resistance to this force.

Considering the above mentioned shortcomings, the following two improvements were made by Zhang, Liu, et al. (2019): (1) Not only the shear resistance of the bond between the steel plate and the old concrete and the one between the old and the new concrete is calculated and designed, but also the radial force resistance is considered. Adhesive anchors are employed to provide the radial force resistance between the steel plate and the old concrete. (2) Steel-fiber reinforced concrete is used to replace the concrete and the steel bar net. This results in a significant decrease of the thickness of the new concrete.

The mechanical behavior of the curved concrete segments, strengthened by the SPCCS strengthening technique with different dimensions of strengthening material layers, was investigated (Zhang, Liu, et al., 2019). It was shown that the SPCCS strengthening technique results in a significant increase of the bearing capacity of the concrete segments. The radial and the shear forces transmitted across the interface

of the strengthened segments and between different material layers were quantified by Zhang, Liu, et al. (2019). This provides a reference for the design of the dimensions of strengthening material layers, used for strengthening of the entire tunnel ring and for the design of the connectors between different material layers.

So far, investigations of segmental tunnel linings strengthened by the SPCCS strengthening technique were described in the literature. Since the load-carrying mechanism, the failure process, and the benefits of strengthening tunnel structures by the SPCCS strengthening technique are unknown, research is needed before application of this technique in practical engineering. A full-scale test of the strengthening of the segmental tunnel ring is described in the present paper. The design of the dimensions of the strengthening material layers and of the connectors at different interfaces are based on the results obtained in previous research (Zhang, Liu, et al., 2019). Pre-analysis was conducted with the help of the numerical model reported in previous research works (Liu, Jiang, Yuan, & Mang, 2018b; Zhao, Liu, Bao, Yuan, & Bai, 2016). The full-scale test is a necessary prerequisite for future model analysis.

2. Experimental program

2.1. SPCCS strengthening technique

The SPCCS strengthening technique is illustrated in Figure 2. In this technique, see Figure 2(a), a curved steel plate is employed as the main strengthening device. Studs, shown in Figure 2(b), are welded to the surface of the steel plate. The L-shaped steel bars, see Figure 2(c), which are fixed to the inner surface of the segmental tunnel lining, are used as shear connectors. Adhesive anchors are pull-out connectors, providing resistance to the radial force between the steel plate and the segmental tunnel lining (*old concrete*). The space between the two is filled with steel-fiber reinforced concrete (*new concrete*), which has a high crack resistance. The steel ring consists of six segments in the form of curved steel plates, which are welded together.

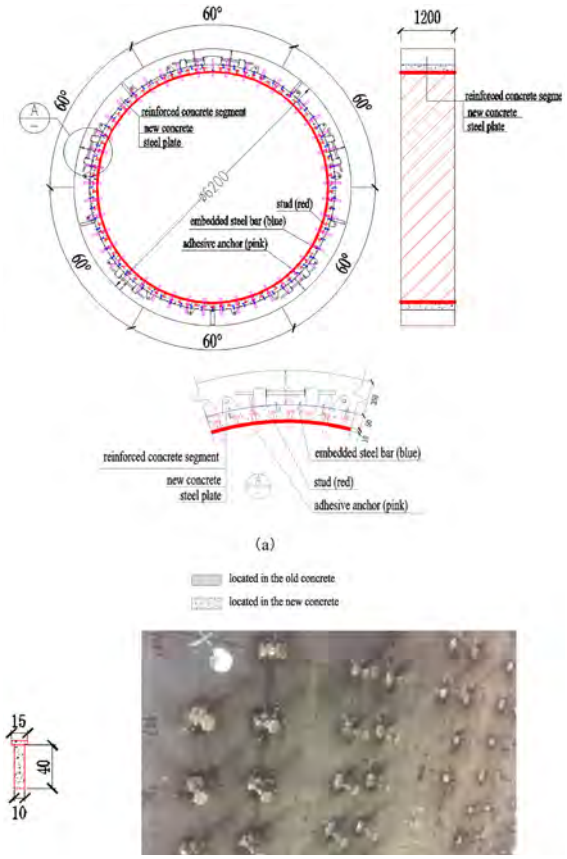

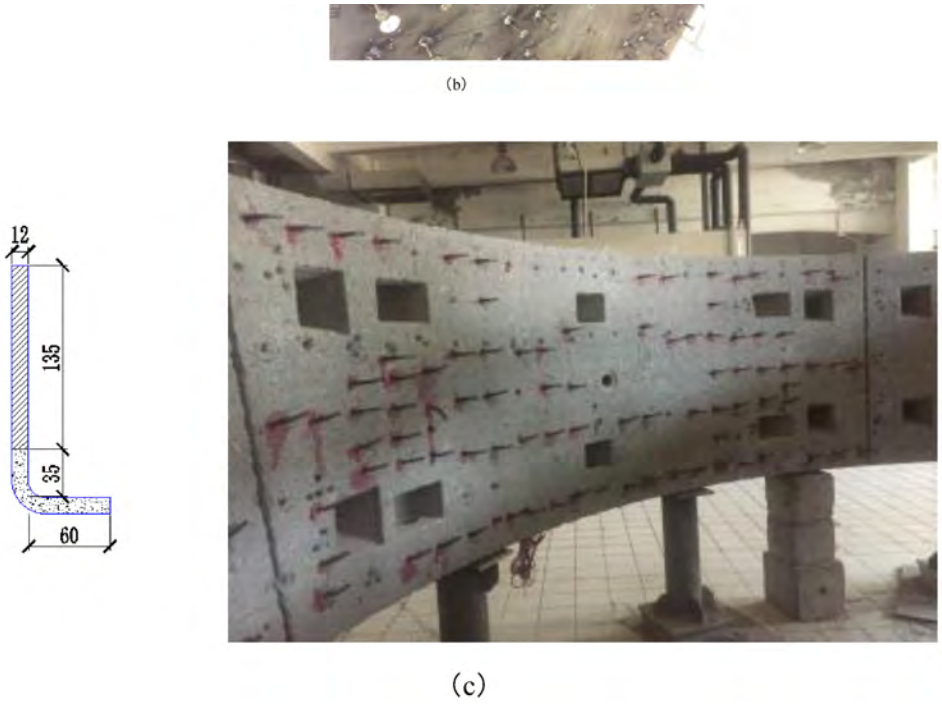

Figure 2. (a) SPCCS strengthening technique (unit: mm); (b) Studs; (c) Embedded steel bars.

Herein, the number of steel segments is equal to the one on the EBSP strengthening technique (Liu et al., 2018a). The following two issues are taken into account: (1) The weight of each steel segment should be small enough to avoid the use of a hoisting machine during construction. (2) The positions of weld joints between adjacent steel segments should not be the same as the ones of the segmental joints of the original tunnel lining. The thickness and the width of the curved plates are 10 mm and 1200 mm, respectively, see Figure 2(a). The central angle of each steel segment is 60°. The segments are welded to a closed ring. The design yield stress of the steel plate is 235 MPa. As shown in Figure 2(b), the diameter and the height of the stud are 10 mm and 40 mm, respectively. The diameter of the stud cap is 15 mm. Its design yield stress is 320 MPa. As presented in Figure 2(c), the L-shaped ribbed steel bars are inserted into the old concrete to provide the shear resistance between the old and the new concrete. The diameter and the design yield stress of the embedded steel bars are 12 mm and 400 MPa, respectively. The depth of insertion of the steel bars in the old concrete is 135 mm, and the length in the new concrete is 35 mm. The length of the bent part of the embedded steel bar is 60 mm. Adhesive anchors are employed to provide resistance to radial tensile stress. Their diameters and their design yield stress are 20 mm and 640 MPa, respectively.

The overall construction process of the SPCCS strengthening technique is as follows: (1) prefabrication of the steel plates including rolling to make them curved, welding of the studs to the outer surface of the steel plate, and drilling holes for the adhesive anchors; (2) roughening of the inner surface of the segmental tunnel lining; (3) construction of the embedded steel bars, including drilling of holes in the old concrete and insertion of ribbed steel bars; (4) installation of steel plates including temporary fixation of six segments inside the tunnel lining, and welding of these segments to obtain a closed ring; (5) construction of adhesive anchors including drilling of holes in the old concrete, insertion of the anchors, and fixation of nuts; (6) pouring of steel-fiber reinforced concrete into the gap between the old concrete and the steel plate.

2.2. Experimental specimen

The non-strengthened segmental tunnel lining employed in this experiment is one that is widely used in the Shanghai rail transit. As shown in Figure 3, it includes six segments, referred to as F, L1, L2, B1, B2, and D. The outer and the inner diameters of the structure are 6200 mm and 5500 mm, respectively. Adjacent segments are connected by bolts. The six segmental joints, are located at 8°, 73°, 138°, 222°, 287°, and 352°. The schematic diagram of the segmental joint is shown in Figure 4. The mechanical behavior of this kind of segmental joints was investigated experimentally and analytically by Li, Yan, Wang, and Zhu (2015a), Li, Yan, Wang, Zhu, and Wang (2015b), and Liu, Zhang, Zhang, and Yuan (2017). These parameters are consistent with the ones in previous research works. The non-strengthened segmental tunnel lining was investigated experimentally (Liu, Bai, Yong, & Mang, 2016; Liu, Jiang, et al., 2017; Liu et al., 2018a), numerically (Zhao et al., 2016; Liu et al., 2018b), and analytically (Jiang et al., 2020; Zhang, Hellmich, Mang, Yuan, & Pichler, 2018; Zhang, Mang, et al., 2019; Zhang et al., 2017). The strengthened structure as used in the experiment, is the one shown in Figure 2. The material properties, obtained from tests, are listed in Table 1.

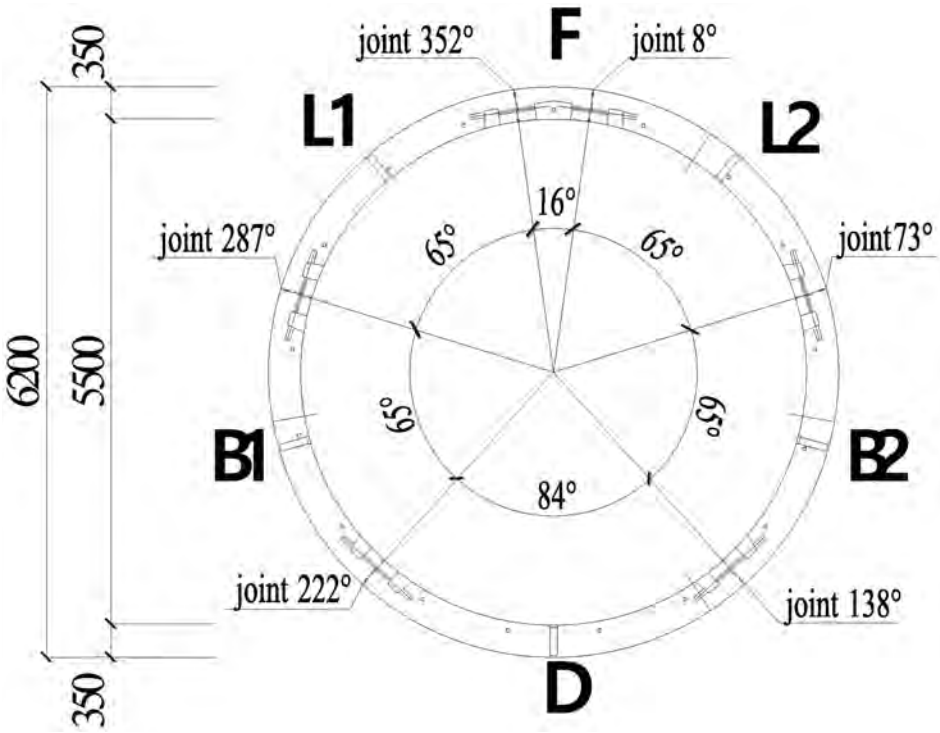

Figure 3. Non-strengthened segmental tunnel lining [mm].

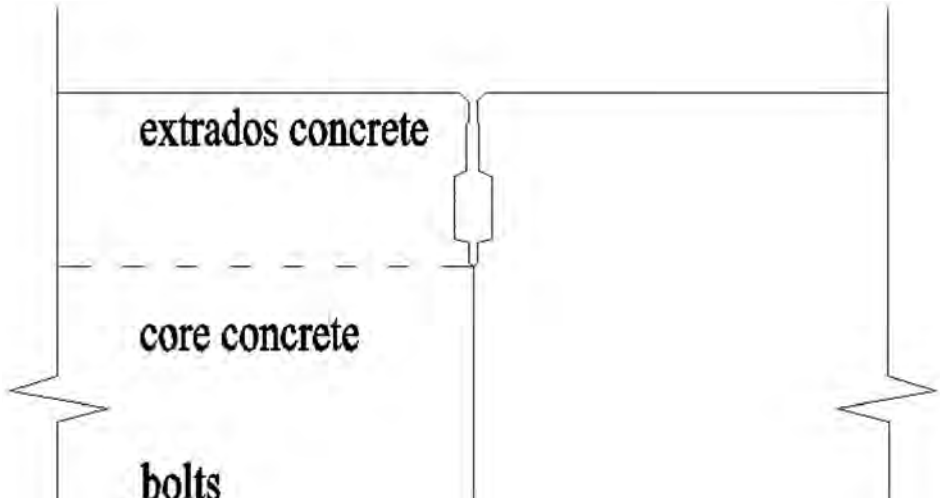

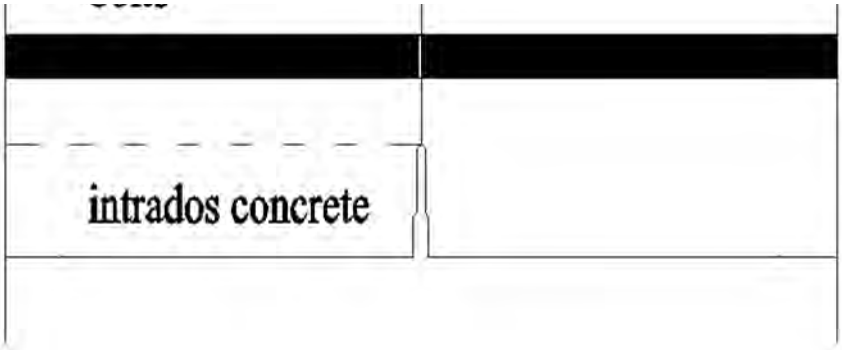

Figure 4. Schematic diagram of a segmental joint (Liu, Zhang, et al., 2017).

Table 1. Material properties. (Table view)

Material type	Young's modulus $[N/mm^2]$	Compressive strength $[N/mm^2]$	Yield stress $[N/mm^2]$
Bolt	2.03×10^5	—	454.85
New concrete	3.13×10^4	67.43	—
Steel plate	1.70×10^5	—	238.22
Embedded steel bars	2.02×10^5	—	281.67

2.3. Loading system

The loading device consists of a self-balanced horizontal loading system, a deformation maintaining system, and a friction reduction system. The self-balance horizontal loading system contains 24 load points, see in Figure 5(a,b). The axis of each point load passes through the center of the system. As shown in Figure 5(c), one load point includes one loading beam, one load holding beam, one jack, and two steel rods. The deformation maintaining system includes load holding beams and nuts, see in Figure 5(c), which can fix the deformation of the structure.

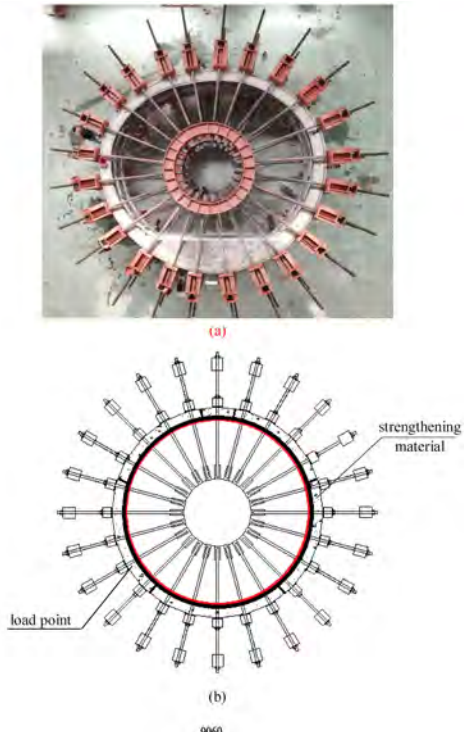

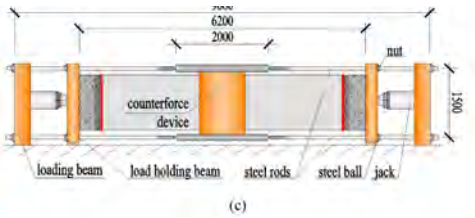

Figure 5. Loading devices: (a) top view photo; (b) top view profile diagram; (c) side view profile diagram (unit: mm).

The characteristic features of this system are as follows: When the structural deformation reaches the strengthening point, the jacks are stopped and the nuts are fixed. The load holding beams, together with the fixed nuts, provides the radial reactive forces to the whole structure in order to maintain the deformation of the structure. After construction of the strengthening technique, the jacks are restarted and the loads are increased to the ones at the strengthening point. Then, the nuts are released, and the loading process is continued. 192 steel balls are deployed between the specimen and the ground to reduce the influence of friction. Such a loading system was employed in many full-scale tests described in previous research (Liu, Bai, et al., 2016; Liu et al., 2018a; Liu, Jiang, et al., 2017).

2.4. Loading process

The 24 point loads are divided into three groups, see Figure 6(a), i.e. six point loads, denoted as P1, ten as P2, and eight as P3. The P1 loads simulate the vertical earth pressure, the P2 loads simulate the horizontal earth pressure, and the P3 loads simulate the loading on the shoulder of the structure. The loading process of the test, consisting of three stages, is shown in Figure 6(b). It is consistent with the one reported in previous research works (Liu et al., 2018a; Liu, Jiang, et al., 2017). The consistency of the loading process allows a comparison of the mechanical behavior of different strengthening techniques. In stage one, P1, P2, and P3 are increased simultaneously. The loads P2 and P3 are defined as follows: $\mathbf{P2 = 0.65\times}$ P1, where 0.65 is the lateral earth pressure coefficient in Shanghai, and $\mathbf{P3 = 0.5 \times (P1 + P2)}$, which results in a smooth distribution of the external loading from the P1 zone to the P2 zone. Stage two starts when P2 has reached the passive earth pressure, the value of which is determined by the soil properties in Shanghai. P2 is then kept constant, while P1 is further increased. P3 is equal to the average of **P1** and **P2.**

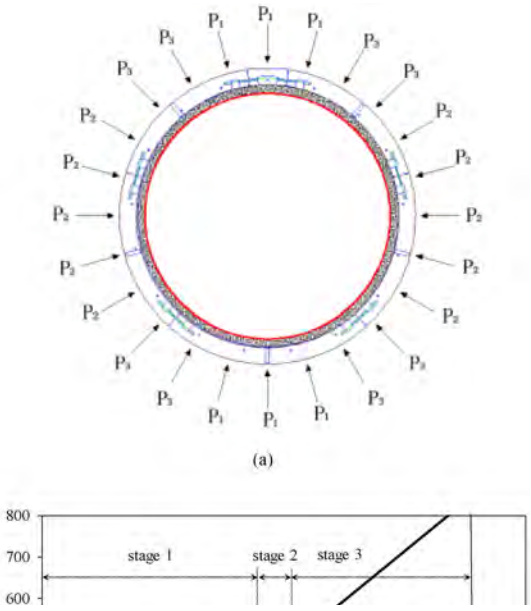

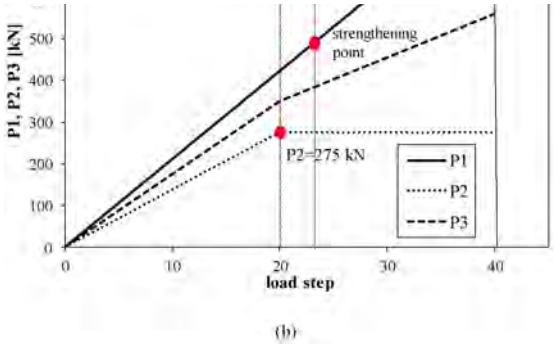

Figure 6. (a) Distribution of point loads; (b) Loading scheme.

When the vertical convergence of the structure reaches 120 mm, referred to as the strengthening point in Figure 6(b), the structural deformation is kept constant by the deformation maintaining system. It is noteworthy that, at the strengthening point, the non-strengthened segmental tunnel lining is close to the ultimate limit state (Liu, Bai, et al., 2016). Outer concrete cracked in compression at 352° segmental joint, and inner concrete cracked in compression at 73° and 287° segmental joints. The bolt at 352° segmental joint yielded in tension. A 120 mm vertical convergence is adopted as the strengthening point in engineering applications. Thereafter, the SPCCS strengthening is installed. Then, stage three starts, where P2 is kept constant while P1 is further increased. P3 is equal to the average of P1 and P2. The third stage ends at failure of the structure.

The design of the loading process is based on the following considerations: (1) The distribution of the loads acting on the tested lining is similar to the external loading, acting on the linings in practical engineering. (2) The internal forces (bending moments and axial forces) of critical cross-sections are equal to those of in actual tunnel structures under operation. Numerous numerical simulations were carried out to ensure it. This design strategy was employed in the tests, on the structure-level, for segmental linings (Blom, 2002; Lu, Lu, and Fan, 2011; Nakamura, Kubota, Furukawa, & Nakao, 2003; Schreyer & Winselman, 2000).

2.5. Measurement program

In the test, the convergences of the structure were measured by cable displacement meters. The strains of the steel reinforcement and of the concrete were measured by strain gauges. They were deployed at the four critical cross-sections, see Figure 7(a), and they were located at 0°, 90°, 180°, and 270°. The strains of the steel plates were measured by strain gauges. They were deployed every 15° along the circumference. The strains of the bolts at the joints were recorded by strain gauges. The outer dilations of the segmental joints were measured by displacement meters, see Figure 7(b), deployed on the outer surface of the six joints. The layout of these displacement meters is shown in Figure 7(a). Besides, the relative tangential slippage and the value of the radial stripping between different material layers were recorded by displacement meters. Information about the sensors at the measurement points and their tasks are listed in Table 2.

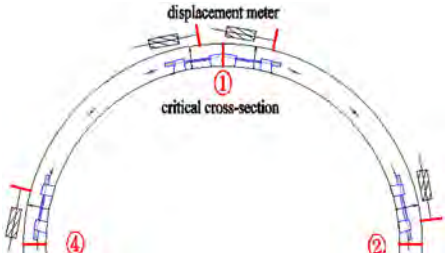

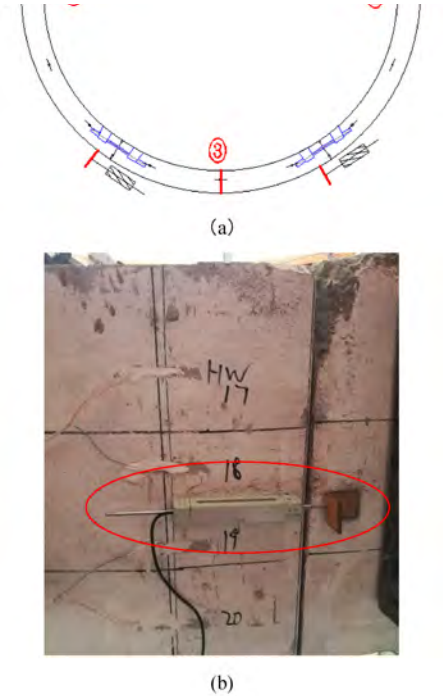

Figure 7. (a) Schematic diagram of layout of critical cross-sections and sensors at the joints; (b) Photo of displacement meter at joints.

Table 2. Sensors at measurement points and their tasks. (Table view)

Test item	Sensor	Range	Precision	Number
Overall deformation	Displacement meter	500 mm	0.01 mm	14
Strain of steel reinforcing	Strain gauge	20,000 με	1 με	136
Strain of bolt	Strain gauge	20,000 με	1 με	12
Strain of concrete	Strain gauge	20,000 με	1 με	136
Joint dilation	Displacement meter	100 mm	0.01 mm	24
Strain of steel plate	Strain gauge	20,000 με	1 με	128
Relative slippage	Displacement meter	100 mm	0.01 mm	24
Relative stripping value	Displacement meter	100 mm	0.01 mm	24

3. Failure process and experimental results

3.1. Failure state

At $\mathbf{P1 = 452kN,}$ the vertical convergence reached the strengthening point. The deformation was kept constant and the construction of the strengthening device was carried out. Thereafter, the test was continued. At P1 = 782kN, a kinematic chain has developed. Hence, the convergences increased rapidly without increase of the external loading. The test was stopped because of the risk of structural collapse. This load level was defined as the failure load. The failure state is shown in Figure 8. The outer concrete at joints 8°, and 352°, and at the position of 180° crushed in compression. The bolt at joint 73° yielded in tension. The steel plate yielded in tension from 345° to 15°, and at 180°. The bond between the old and the new concrete failed from 328° to 13°, and from 162° to 210°.

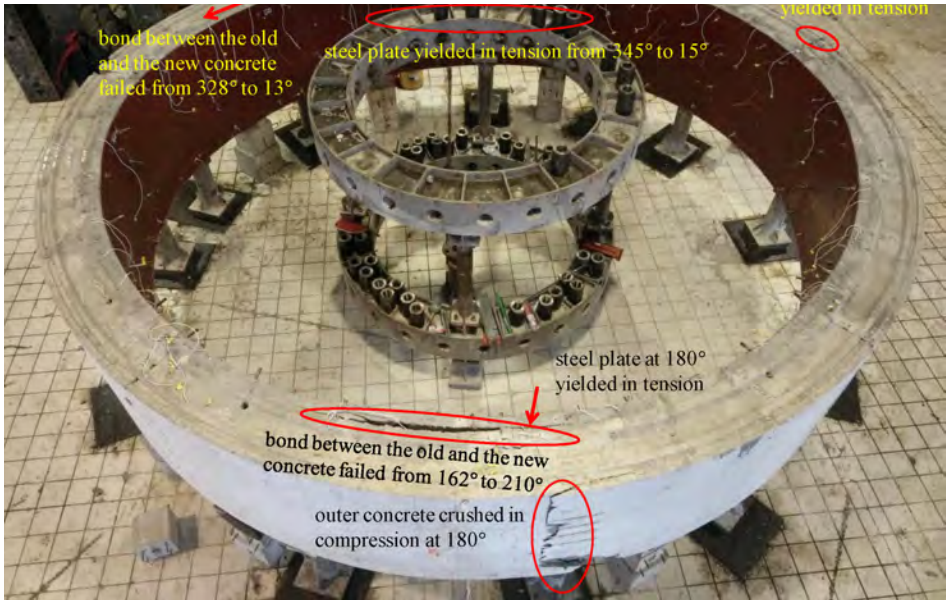

Figure 8. Failure state of the segmental tunnel lining, strengthened by the SPCCS technique.

3.1.1. Cracking and failure of segments

Two phenomena were observed at concrete segments. One is cracking in tension, and the other one is crushing in compression. At the non-strengthened stage, no cracks were observed on the outer surface of the structure. At $\mathbf{P1 = 430kN,}$ a crack occurred at 176° on the inner surface of the structure. At $\mathbf{P1 = 452kN,}$ i.e. at the strengthening point, its width increased to 0.05 mm, see Figure 9(a). After the structure was strengthened, the load was further increased. At $\mathbf{P1 = 462kN,}$ cracks occurred on the outer surface of the structure at 90° and 270°. Their widths were 0.02 mm.

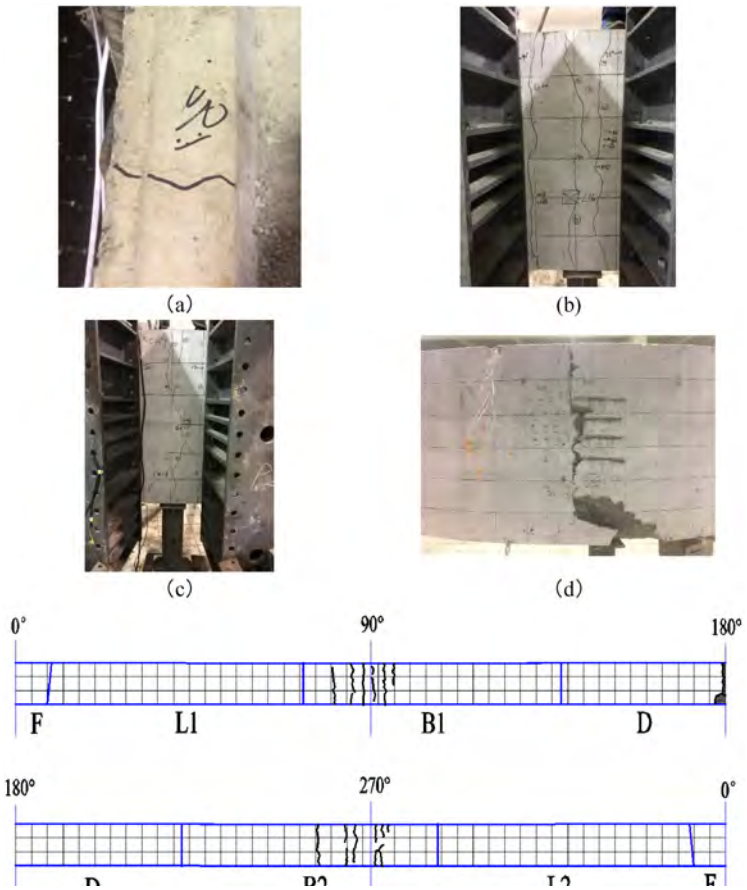

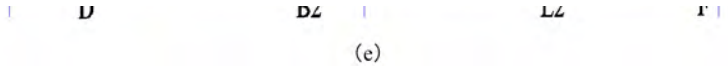

Figure 9. Cracking and failure of segments: (a) crack at 176°; (b) cracks at 90°; (c) cracks at 270°; (d) concrete failure at 180°; (e) distribution of segment failure.

With increasing load, additional cracks developed in the vicinity of these two positions. The distributions of the cracks around 90˚ and 270˚ at the failure state, i.e. at $\mathbf{P1 = 782kN,}$ are shown in Figure 9(b,c). The maximum crack widths are 0.50 mm and 0.25 mm, respectively. In both regions, the average crack distance is 200 mm. At this load intensity, the outer concrete, at the 180˚ position, failed in compression, see Figure 9(d). The distribution of segment failures is shown in Figure 9(e), where the black solid lines represent the crack. The shaded area refers to the position of failure in compression.

The cracks on the inner surface of the segmental tunnel lining could not be observed because of being hidden by the steel plate and the new concrete. The strengthening material significantly reduces the durability problem, caused by inner surface cracks, so long as the bond between different material layers is intact. It is mentioned that bond failure, resulting in significant radial stripping occurred only after the structure has reached the ultimate limit state (ULS). Hence, the hiddenness of these cracks is no real problem before the strengthened structure has reached the ULS.

3.1.2. Joint failure

In the test, the joints 73˚ and 287˚ were subjected to a combination of a compressive axial force and a negative bending moment, and the rest of them were subjected to a combination of a compressive axial force and a positive bending moment. The modes of failure of the segmental joints were observed and recorded during the test. At the non-strengthened stage, at $\mathbf{P1 = 421kN,}$ the outer concrete at joint 352˚ split in compression. At $\mathbf{P1 = 438kN,}$ splitting in form of small compression cracks of the inner concrete occurred at joints 73˚ and 287˚**.** After strengthening of the structure, the load was further increased.

Photos of all joints when the strengthened structure reached the failure state are shown in Figure 10. The outer concrete at joint 8˚ and joint 352˚ crushed in compression and fell down, the inner compression cracks at joint 73˚ and joint 287˚ did not grow much, joint 138˚ remained intact, and the outer concrete at joint 222˚ cracked in compression. The form of damage of the joints at 8° and 352°, which is crushing of the outer concrete, agrees well with the results from the pre-analysis, where a 2D nonlinear numerical model, validated by other full-scale tests (Liu et al., 2018b; Zhao et al., 2016), was employed.

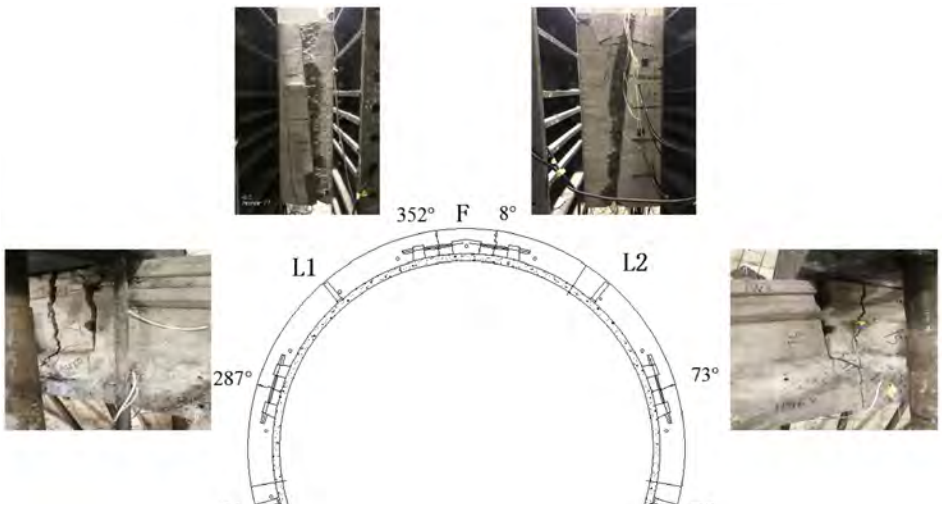

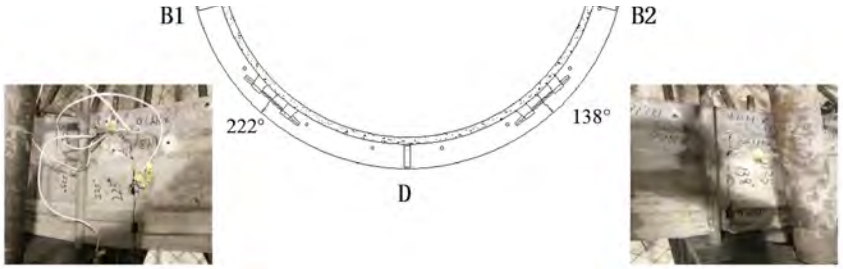

Figure 10. Damage of joints at the failure state.

In this model, a segmental joint is simulated by a collection of nonlinear springs and two rigid beam elements, see Figure 11(a). These elements simulate the interfaces at the joints, while a series of compressive springs simulates the contact at the interfaces. The bolt connecting adjacent segments is simulated by a nonlinear spring element. In the simulation, damage of the joints is assumed to occur if the stress in the extrados area, shown in Figure 4, becomes equal to the compressive strength. The P1 – compressive stress diagram in the extrados area, at joint 8°/352°, is illustrated in Figure 11(b). It is shown that, for P1 = 654kN the concrete stress in the extrados area reaches the compressive strength.

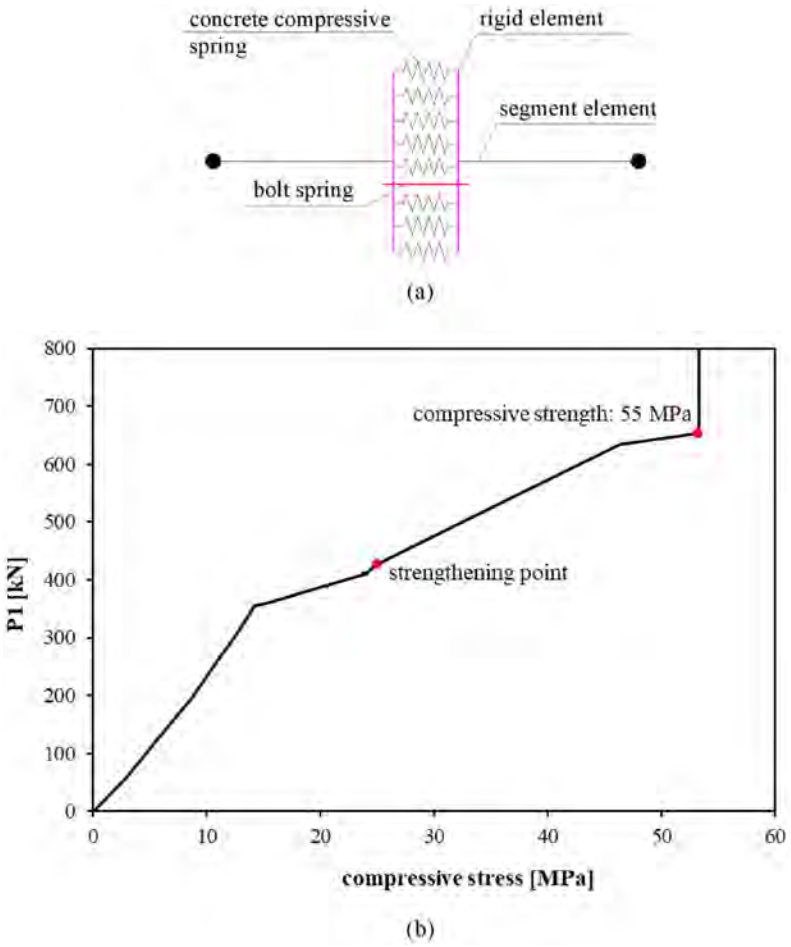

Figure 11. Numerical pre-analysis: (a) segmental joint model; (b) evolution of extrados concrete at joint 8°/352°.

3.1.3. Damage of the bond

There are two kinds of bond in the SPCCS strengthening technique. One of them is the bond between the steel plate and the new concrete, while the other one is the bond between the new and the old concrete. In

the test, the dominant failure mode is failure of the bond between the new and the old concrete, see Figure 12. Radial stripping between the steel plate and the new concrete occurred from 345° to 15°. The maximum stripping value was only 3.38 mm. Radial stripping between the old and the new concrete occurred from 328° to 13°, and from 162° to 210°. The maximum stripping value was 28.92 mm.

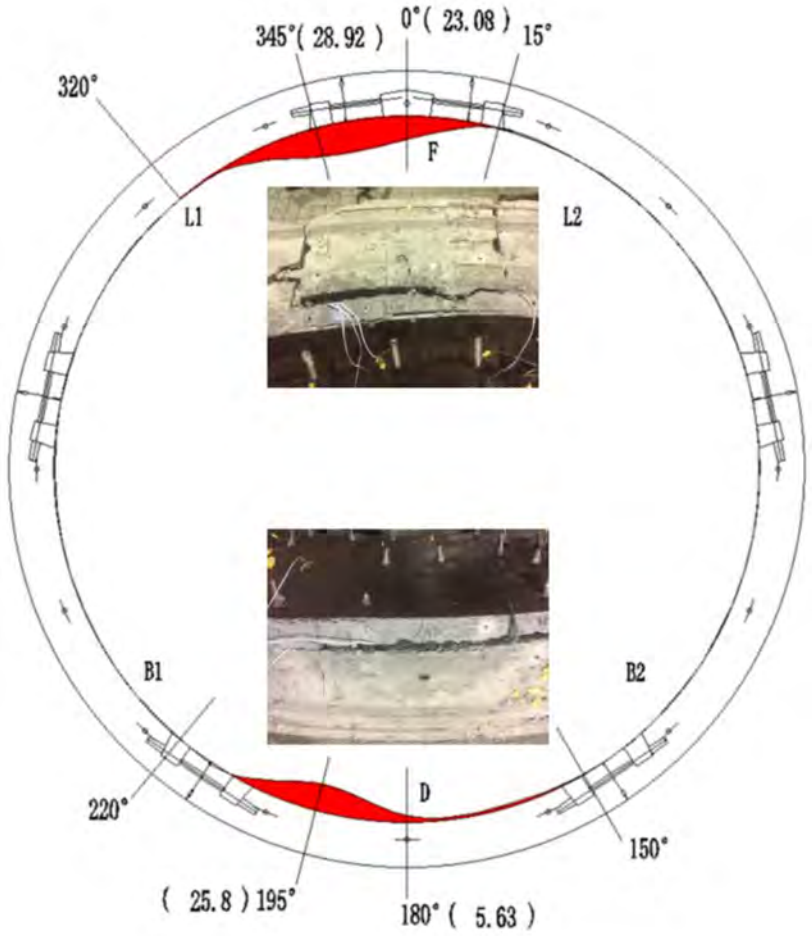

Figure 12. Damage of bond at the failure state (unit: mm).

The failure mode was pull-out of the adhesive anchor from the concrete segment. The adhesive anchor did not fail in tension. No tangential slippage was observed in the test. As described in previous research (Zhang, Liu, et al., 2019), stripping is the dominant bond failure of the curved beam. The radial force was obtained from:

$$\sigma_r = \frac{h_s}{R}\sigma, \tag{1}$$

where σ_r is the radial stress of the bond, h_s denotes the thickness of the steel plate, R is the radius of the curved beam, and σ stands for the axial stress of the steel plate.

The tensile radial stress of the bond is denoted as positive while the compressive radial stress is denoted as negative. The tensile radial stress results in stripping of the bond. In the full-scale test, the top and the bottom of the structure were subjected to a combination of axial force and positive bending moment. Hence, the steel plate was in tension. On the contrary, the steel plate at the waist of the structure was in compression. Stripping of the bond is distributed in the top and bottom area of the bond, which

agrees well with the results obtained by Equation (1).

3.2. Failure process and failure mechanism

The load – vertical convergence diagram resulting from the test is shown in Figure 13. The failure process before strengthening of the lining has been obtained in previous research (Liu, Bai, et al., 2016; Liu et al., 2018a; Liu, Jiang, et al., 2017). The failure process after strengthening is described in the following: (1) at first, the outer concrete at joint 352˚ crushed; (2) thereafter, the steel plate yielded in the region from 352˚ to 0˚; (3) then, the bolt at joint 73˚ was yielding; (4) next, the outer concrete crushed at joint 8˚; (5) thereafter, the steel plate yielded at 15˚; (6) then, the steel plate yielded at 180˚, after the steel reinforcement at this position had already yielded; (7) this was followed by crushing of the concrete at 180˚; (8) finally, the steel plate yielded at 345˚.

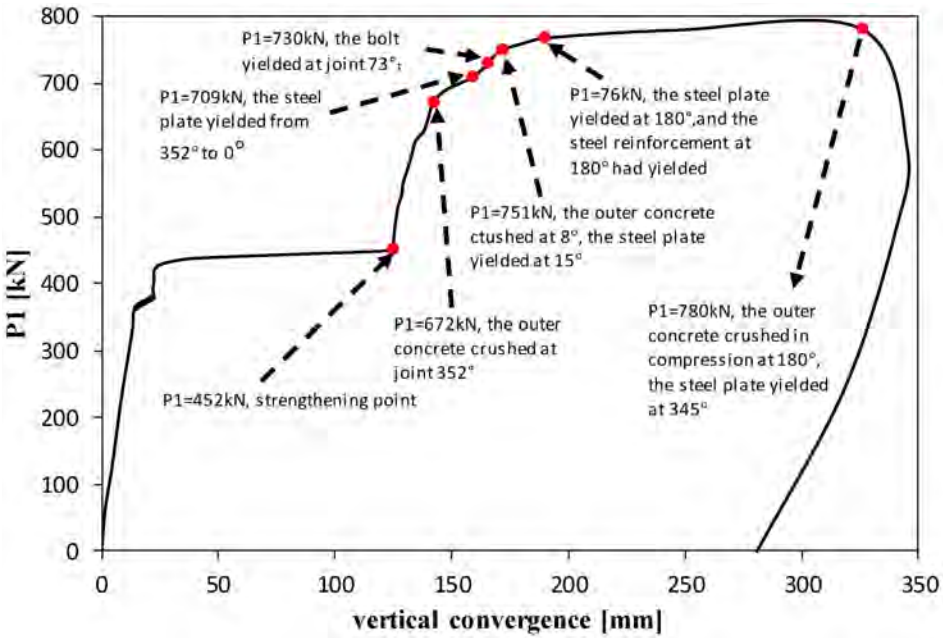

Figure 13. Load – vertical convergence of segmental tunnel lining strengthened by the SPCCS technique.

The cross-sections of the strengthened structure are subjected to bending moments and compressive axial forces. There are six main categories of cross-sections of the strengthened structure, see Figure 14: (a) the materials in the compressive zone are concrete and reinforcing steel, while the materials in the tensile zone are the steel of the plate and of the reinforcement; (b) the materials in the compressive zone are the concrete, the steel of the plate and of the reinforcement, while the material in the tensile zone is the steel of the reinforcement; (c) the material in the compressive zone is the concrete, while the materials in the tensile zone are the steel of the plate and the bolt; (d) the materials in the compressive zone are concrete and steel of the plate, while the material in the tensile zone is the steel of the bolt; (e) all materials of the cross-section of the composite segment are in the compressive zone; (f) all materials of the cross-section of the composite segmental joint are in the compressive zone.

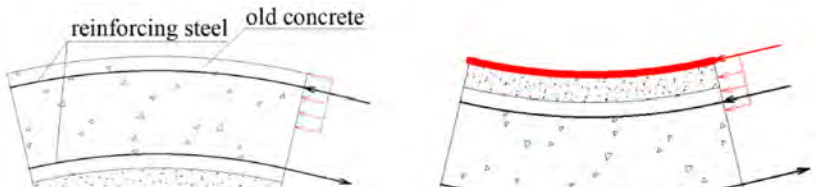

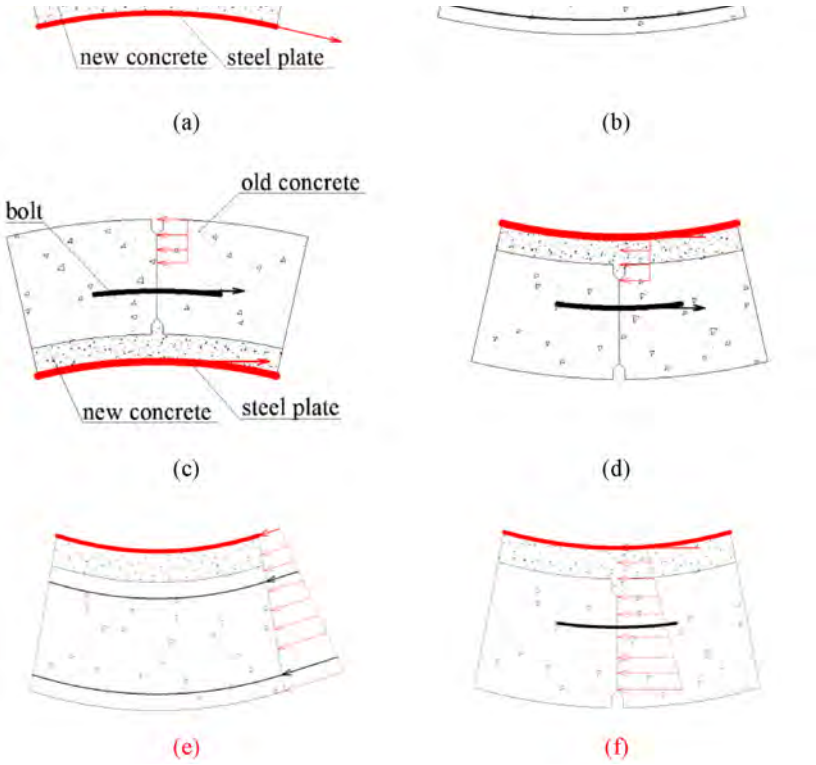

Figure 14. Six categories of cross-sections.

When materials fail either in the compressive or the tensile zone, the stiffness of the cross-section decreases rapidly, resulting in a plastic hinge. Herein, materials failure in the compressive zone means that concrete is crushing or steel is yielding in the segment or at the joint. Material failure in the tensile zone means that the steel of the bolt or of the plate is yielding. Crushing of concrete was observed in the test, while yielding of steel follows from the test data.

The failure mechanism of the segmental tunnel lining, strengthened by the SPCCS technique, is characterized by a high degree of ductility. The failure process can be divided into three stages, i.e. the elastic stage, the elasto-plastic stage, and the plastic stage. At $\mathbf{P1 = 672kN,}$ the outer concrete crushed in compression at joint 352°. The first plastic hinge occurred at this cross-section, which belongs to category (c). The structure entered into the elasto-plastic stage. This load level represents the elastic limit. At $\mathbf{P1 = 730kN,}$ the bolt at joint 73° yielded, resulting in the second plastic hinge. This situation refers to category (d) of cross-sections. At $\mathbf{P1 = 751kN,}$ the outer concrete at joint 8° crushed in compression. This situation refers to category (c) of cross-sections. It led to the third plastic hinge. At $\mathbf{P1 = 768kN,}$ the steel of both the plate and the reinforcement at 180° were yielding. This situation refers to category (a) of cross-sections. It resulted in the fourth plastic hinge. At this load level, the structure entered into the plastic stage.

Originally, the strengthened structure was statically indeterminate to the third degree. Hence, its degree of freedom (DOF) is equal to -3. When three plastic hinges occurred, the structure became a statically determinate structure. Consequently, the DOF is equal to zero. When the fourth plastic hinge occurred, the DOF of the structure became equal to 1, and a kinematic chain developed in the strengthened structure. The load level, at which the fourth plastic hinge occurred, is defined as the bearing capacity limit. When it was reached, the structure did not immediately collapse. It was able to carry a slightly higher load, because it was surrounded by the horizontal loading system, which provided support to the structure. However, the deformations increased rapidly, and several parts of the steel plate yielded. After the outer concrete at 180° crushed in compression, the structure failed. The vertical

convergence reached 324 mm.

3.3. Experimental results

3.3.1. Structural deformation

The cross-section of the deformed structure is similar to an ellipse, see Figure 15. The top and the bottom of the structure deformed inward, while the waist of the tunnel deformed outward. At the strengthening point ($\mathbf{P1 = 452kN}$), the vertical convergence was 125 mm. This value differs by 4% from that in the design of the test, i.e. 120 mm. The horizontal convergence was 105 mm. At the elastic limit ($\mathbf{P1 = 672kN}$), the vertical and the horizontal convergences were 142 mm and 119 mm, respectively. At the bearing capacity limit, i.e. at $\mathbf{P1 = 768kN,}$ the vertical and the horizontal convergence were 190 mm and 150 mm, respectively.

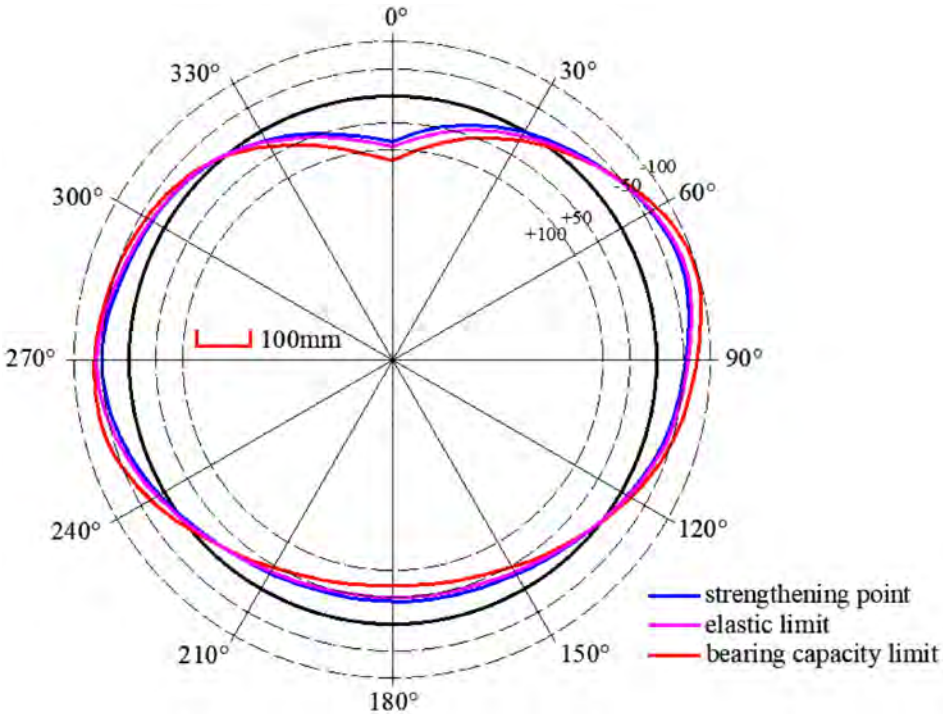

Figure 15. Overall structural deformation (unit: mm).

3.3.2. Opening of joints

After strengthening of the structure, the inner joint was covered by the steel plate and the new concrete. Hence, only the dilations at the outer joints could be measured. Load − opening curves of joints are shown in Figure 16. A positive value means closure of the joint, whereas a negative value indicates its opening. At two of the six joints, namely, at joints 73° and 287°, the outer joint opened in the test. At the remaining four joints, the outer joint closed. It follows from Figure 16 that the joint stiffness increased after strengthening of the structure. At the load levels $\mathbf{P1 = 672kN,}$ $\mathbf{P1 = 730kN,}$ and $\mathbf{P1 = 751kN,}$ the outer concrete at joint 352° crushed in compression, the bolt at joint 73° yielded, and the outer concrete at joint 8° crushed in compression, respectively. All of this resulted in a decrease of the joint stiffness.

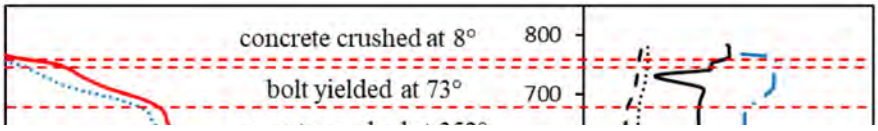

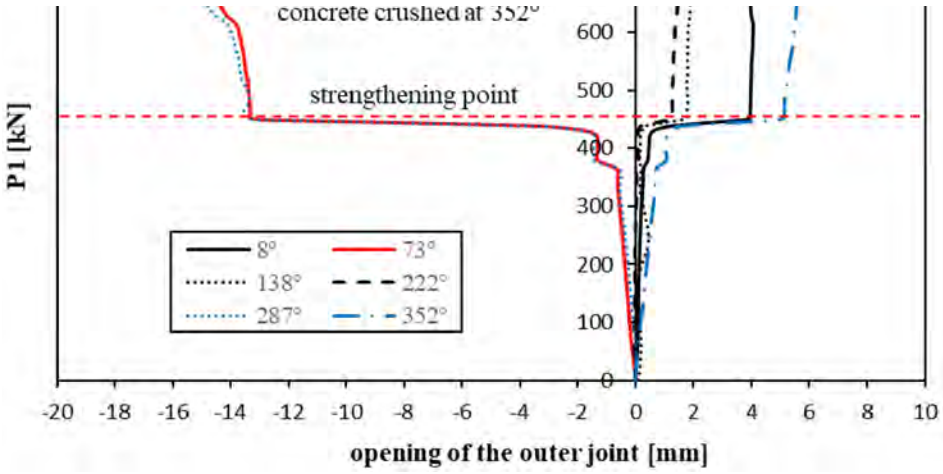

Figure 16. Load - joint opening curves.

3.3.3. Bolt strain

Before reaching the strengthening point, the bolt strain increased with increasing of the load, see Figure 17. At the strengthening point, the bolt at joint 352˚ **yielded.** After strengthening, as the load continued to increase, the bolt at joint 73˚ yielded. The development of the bolt strain at joint 8° and 287° is not shown in Figure 17, because the strain gauges were broken during the test.

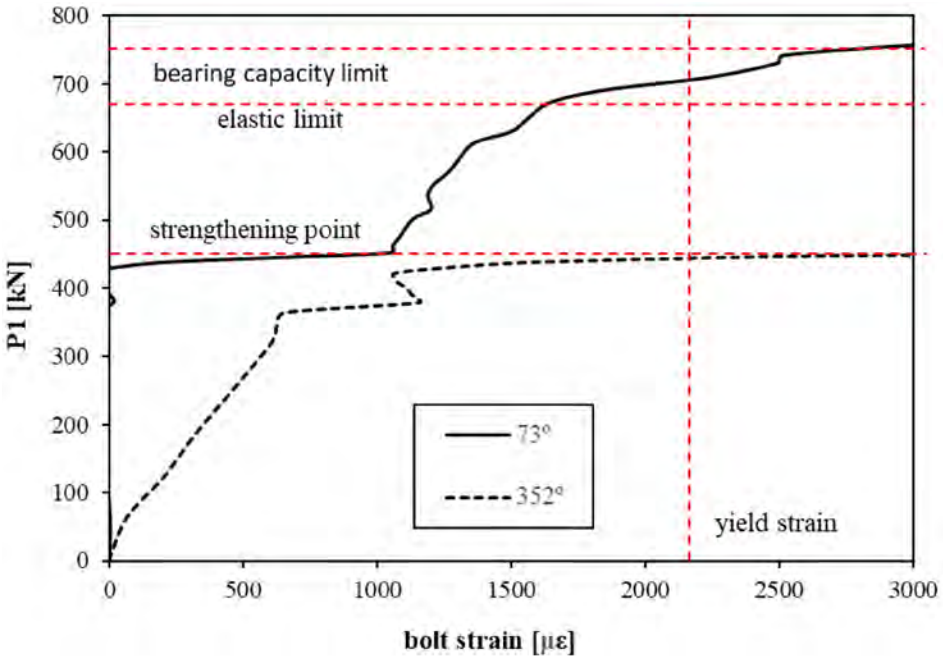

Figure 17. Load – bolt strain curves.

3.3.4. Stress of the steel plate

The stress of the steel plate increased from zero at the strengthening point. The distribution of this stress at the bearing capacity limit (**P1 = 768kN**) is shown in Figure 18. At the top and the bottom of the cross-section, the strain in the steel plate is tension. The yield stress, i.e. 238.22 MPa, was reached at the 0˚**,** the 180˚**,** and the 352˚ position. At the waist of tunnel, the strain in the steel plate is compression. The maximum compressive stresses are located at joints 73˚ and 287˚**.** The maximum value of the stress is 81% of the yield strength.

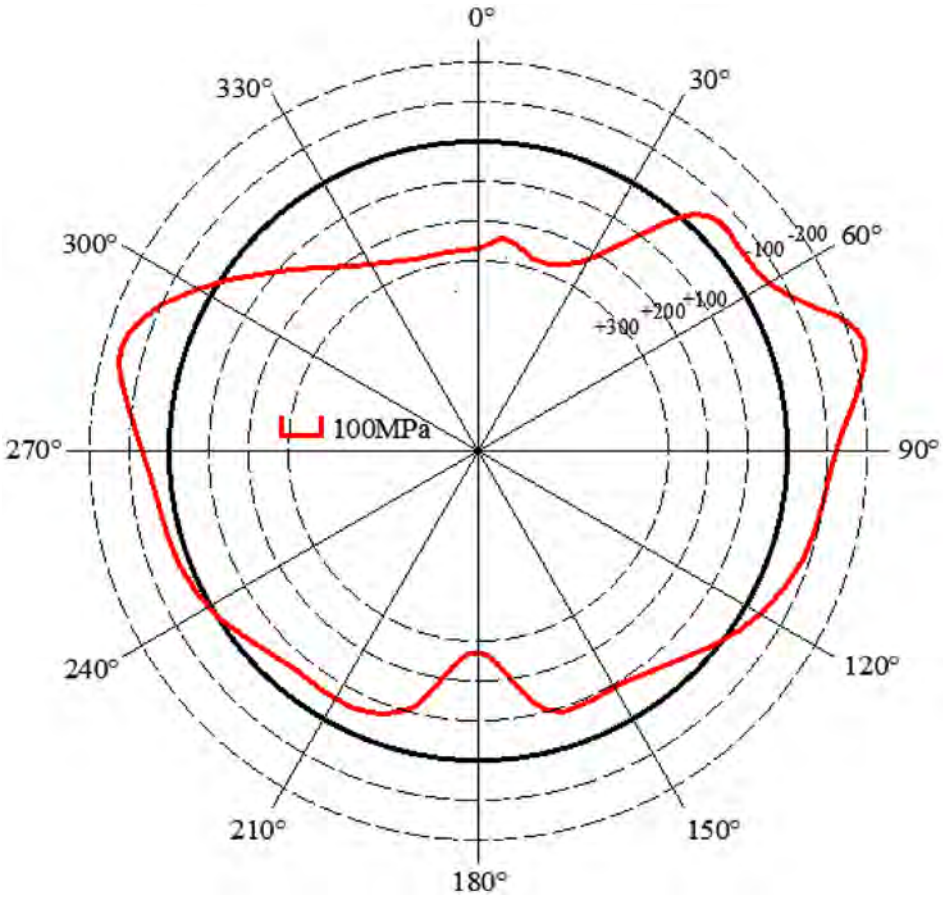

Figure 18. Distribution of the stress of the steel plate at the bearing capacity limit (unit: MPa).

3.3.5. Relative slip and stripping value of the bond

In the SPCCS technique, there are two kinds of interfaces (as was mentioned in Section 3.1.3). The tangential slippage and the radial stripping value of both interfaces were measured in the test. The data at the bearing capacity limit are listed in Table 3. A negative value of slippage means that the steel plate moved in the anti-clockwise direction relative to the new concrete, or the new concrete moved in the anti-clockwise direction relative to the old concrete. The stripping value is always positive.

Table 3. Slippage and stripping values of the interfaces between the steel plate and the new concrete, and between the new concrete and the old concrete at the bearing capacity limit. (Table view)

Angle	Interface between the steel plate and the new concrete		Interface between the new concrete and the old concrete	
	Slippage [mm]	Stripping [mm]	Slippage [mm]	Stripping [mm]
		Top		
287	0.00	0.00	−0.39	0.00
320	−0.05	0.00	0.04	0.00
352	0.37	0.50	−0.58	5.10
0	0.00	1.68	0.00	2.30
8	2.01	0.32	−0.43	0.34
40	−0.02	0.00	−0.07	0.00
73	0.12	0.28	−0.09	0.00
		Bottom		
105	0.26	0.01	0.04	0.00

Angle	Interface between the steel plate and the new concrete		Interface between the new concrete and the old concrete	
	Slippage [mm]	Stripping [mm]	Slippage [mm]	Stripping [mm]
138	−0.10	0.09	0.08	0.00
180	−0.17	0.01	−0.38	3.58
222	−0.01	0.05	−4.15	0.90
255	−0.06	−0.03	−0.01	0.00

Generally, at the bearing capacity limit, slippage and stripping occurred in the top and the bottom region of the strengthened structure. The values of these quantities are very small. Predominantly they appeared at the interface between the old and the new concrete. The maximum slippage and the maximum stripping value between the new and the old concrete are −4.15 mm and 5.10 mm. They occurred at 222° and 352°, respectively.

4. Comparison between SPCCS strengthening and EBSP strengthening

4.1. Brief introduction of a full-scale test using the EBSP strengthening technique

A full-scale test was conducted on the deformed segmental tunnel lining strengthened by the EBSP strengthening technique (Liu et al., 2018a). In this technique, the steel plate is employed as strengthening element, and the bond between the steel plate and the segmental tunnel lining is established by epoxy. In the EBSP strengthening test, the non-strengthened tunnel lining and the loading process are the same as the ones in the test reported in the present paper. The strengthened structural failure is initiated by the brittle failure of the bond between the steel plate and the original structure. At the failure state, the outer concrete at 8° and 222° failed in compression, and the bond between the steel plate and the original concrete failed from 330° to 45° and from 170° to 255° (Liu et al., 2018a). Two strengthening techniques will be compared, with respect to the failure mechanism, the strengthening benefits, the stress in the steel plate, the joint opening, the bolt strain, slippage, and the stripping value.

4.2. Failure mechanism

A comparison between the load – vertical convergence curve based on the SPCCS strengthening technique and the one, based on the EBSP strengthening technique (Liu et al., 2018a), are shown in Figure 19. The performance points ①–⑥ in the SPCCS test refers to the following situations: ① the strengthening point, ② crushing of the outer concrete at joint 352° (the location of the first plastic hinge), ③ yielding of the bolt at joint 73° (the location of the second plastic hinge), ④ crushing of the outer concrete at joint 8° (the location of the third plastic hinge), ⑤ yielding of the steel plate and of the reinforcement at 180° (the location of the fourth plastic hinge), and ⑥ the failure point. The performance points ①–③ in the EBSP test refer to the following situations: ① the strengthening point, ② failure of the bond between the concrete and the steel plate in the range of 8° to 40°, and ③ the failure point. Comments on these curves are listed in Table 4.

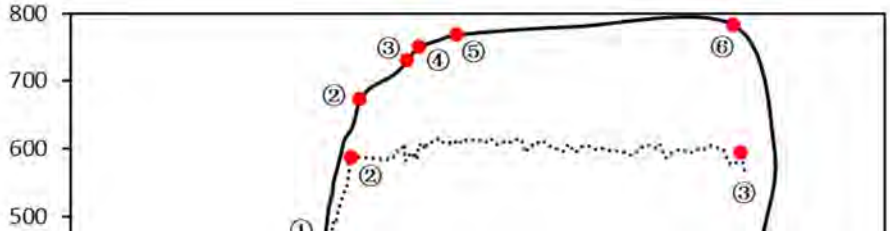

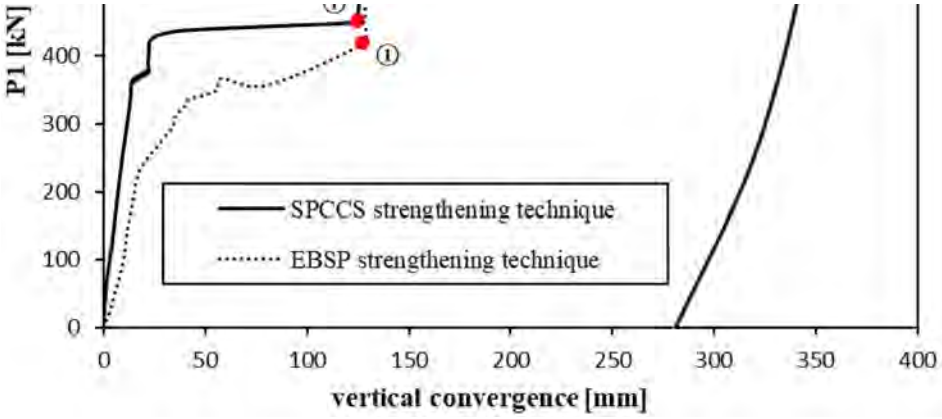

Figure 19. Comparison of the load – vertical convergence curve based on the SPCCS strengthening technique and on the EBSP strengthening technique.

Table 4. Comparison of failure modes of two different strengthening techniques. (Table view)

		Strengthening point	Elastic limit	Elasto-plastic stage		Bearing capacity limit	Plastic stage
SPCCS strengthening	Number	①	②	③	④	⑤	⑥
	Load [kN]	452	672	730	751	768	782
	Vertical convergence [mm]	125	142	166	172	190	325
EBSP strengthening	Number	①	②				③
	Load [kN]	418	586				594
	Vertical convergence [mm]	127	138				329

The failure mechanism of the structure, strengthened by the EBSP strengthening technique, is less ductile. The failure process only contains two stages, i.e. the elastic stage (①–②) and the plastic stage (②–③). The reason for that is the brittleness of the failure mode of the bond between the steel plate and the concrete segment, established by the epoxy. Failure of the strengthened structure is initiated by the bond failure. Thus, after the bond has failed, the steel plate ring cannot act in combination with the original structure. This results in loss of stiffness of the structure, which rapidly enters into the plastic stage.

The failure mechanism of the structure strengthened by the SPCCS technique is more ductile than the one resulting from the EBSP technique. As described in Section 3.2, the failure process contains three stages, i.e. the elastic stage (①–②), the elasto-plastic stage (②–⑤), and the plastic stage (⑤–⑥). The reason that the failure mechanism of the strengthened structure consists of three stages is that the bond, established by a combination of studs, embedded steel bars, adhesive anchors, and steel fiber reinforced concrete, has high strength and ductility. It ensures that the strengthening material elements work together with the original structure during the whole loading process. Since the structure was originally statically indeterminate to the third degree, the failure process consisted of the successive development of four plastic hinges.

4.3. Steel plate stress

The distributions of the steel plate strain according to the two strengthening techniques at the bearing capacity limit are shown in Figure 20. The bearing capacity in case of SPCCS strengthening and EBSP strengthening are $\mathbf{P1 = 768kN}$ and $\mathbf{P1 = 586kN,}$ respectively. At the top and the bottom of the structure, the strain in the steel plate reaches the yield stress in case of SPCCS strengthening, whereas it is only 27% and 46% of the yield stress at the top and the bottom of the structure in ESBP strengthening. As for the waist of tunnel, the maximum values of the strain in the steel plate are located at joints 73˚ and 287˚. However, none of them reaches the yield stress.

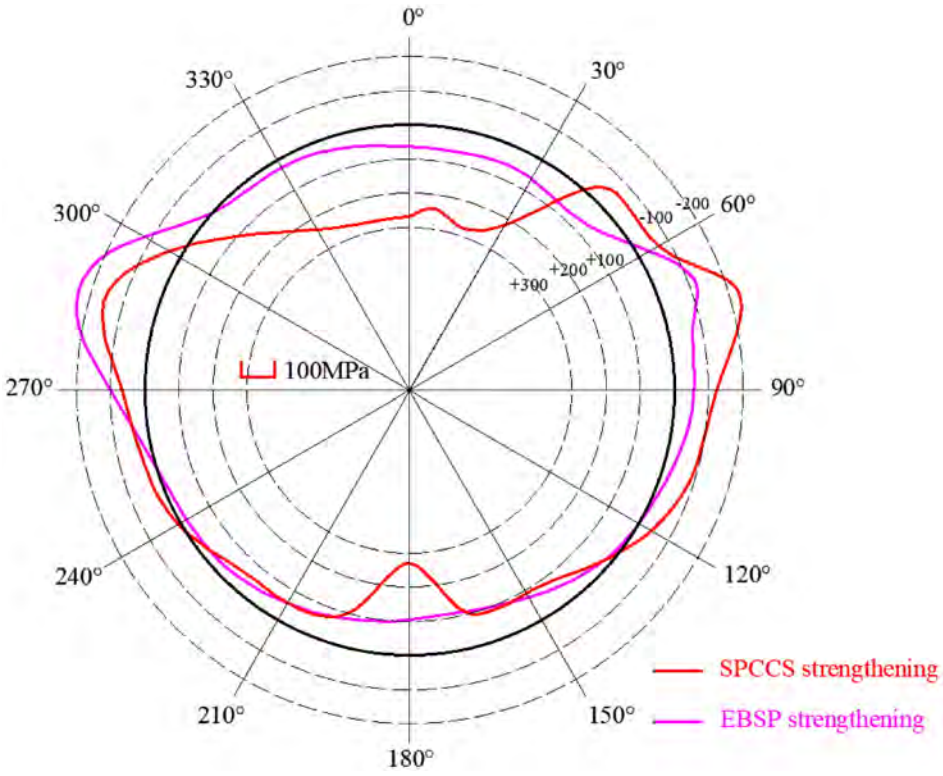

Figure 20. Comparison of the distributions of the strain in the steel plate for two different strengthening techniques (unit: MPa).

As for a segmental tunnel lining, the top area is the critical zone. Hence, this area is the key point of the present research. The utilization rate in the top area in SPCCS strengthening is 3.72 times to that in EBSP strengthening. The reason for this is that the bond between the steel plate and the tunnel lining in SPCCS strengthening is stronger than the one in EBSP strengthening, which ensures that the steel plate is acting together with the original structure during the entire loading process rather than being separated from the lining in advance.

4.4. Joint opening and bolt strain

The bolts connect adjacent concrete segments at their joints. The bolt strain is very relevant to the opening of the joint. The values of these quantities relative to one at the strengthening point are normalized such that the largest value is equal to 1. The bolt strain and the joint opening at 73˚ in SPCCS strengthening, and these quantities at 287˚ in EBSP strengthening are chosen for comparison. The sensors measuring bolt strain at joint 287˚ in SPCCS and at joint 73˚ in EBSP strengthening broke during the test. Considering the symmetry of these two joints, the data at 73˚ and 287˚ are comparable.

The results are shown in Figure 21. The bolt strain is consistent with the joint opening, and the stiffness of the joint in SPCCS strengthening is greater than that in the EBSP strengthening technique.

The thickness of the steel plate and the new concrete in SPCCS strengthening are 10 mm and 50 mm, respectively. The thickness of the concrete segment is 350 mm, see Figure 3. Hence, the thickness of the structural cross-section is 410 mm after strengthening. In EBSP strengthening, the thickness of the steel plate is 20 mm and that of the epoxy can be neglected. Similarly, the thickness of the structural cross-section is 370 mm after strengthening. The inertia moments of the cross-sections at the segmental joint positions in the SPCCS strengthening technique are larger than that in the EBSP strengthening technique. This makes the joints in SPCCS strengthening stiffer.

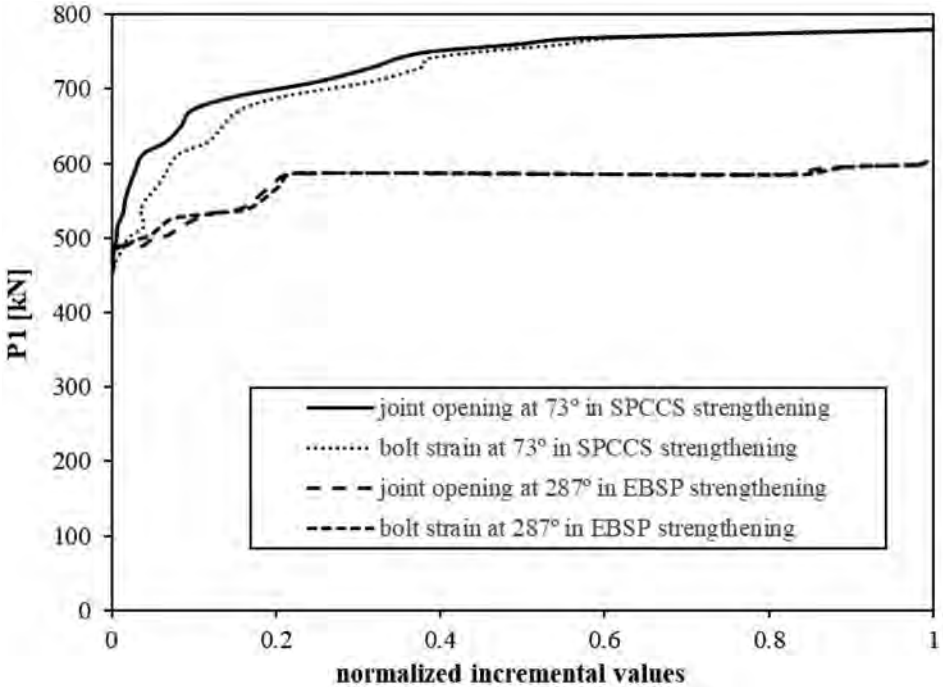

Figure 21. Comparison of joint opening and of bolt strain between two different strengthening techniques.

4.5. Slippage and stripping value of the bond

As mentioned in Section 3.3.5, there are two kinds of interfaces in SPCCS strengthening, slippage and the stripping value, both of which were measured in the test. In EBSP strengthening, there are also two kinds of interfaces, namely, the interface between the steel plate and the epoxy, and the one between the epoxy and the concrete segment. However, because the thickness of the epoxy layer is very small, the sensors could not be deployed. For that reason, only slippage and the stripping value between the steel plate and the concrete segment were measured in the test. For comparison, the measured values of the two interfaces in SPCCS strengthening are superimposed. The distributions of slippage and of the stripping value of the two strengthening techniques at the bearing capacity limit are shown in Figure 22. As for slippage, the area inside the circle means that the steel plate moves in the anti-clockwise direction.

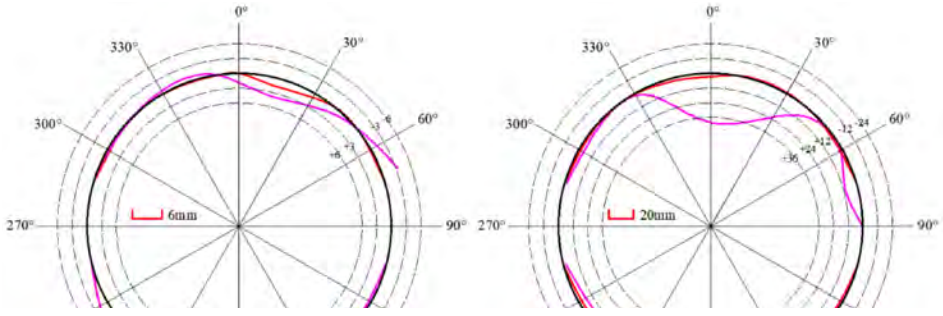

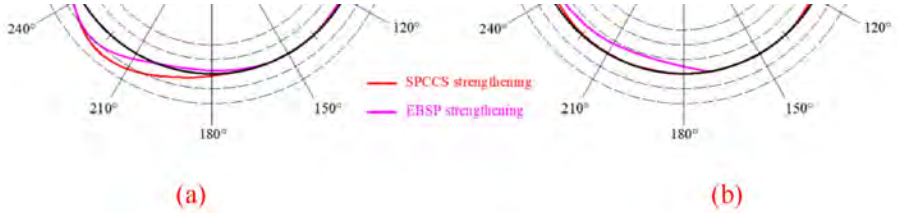

Figure 22. Comparison of the distributions of bond failure for two different strengthening techniques: (a) slippage; (b) stripping valu.

Slippage in both strengthening techniques is very small. While stripping in the SPCCS strengthening technique at the bearing capacity limit is very small, it is large in the EBSP strengthening technique. The reason for that is the higher strength and ductility of the bond in SPCCS strengthening than in EBSP strengthening. At the bearing capacity limit state, the bond in SPCCS strengthening still performs well, whereas in EBSP strengthening it fails all of a sudden and stripping develops quickly.

4.6. Strengthening benefits

The strengthening benefits are the higher bearing capacity, the greater structural stiffness, the larger degree of ductility of the strengthened structure than that of non-strengthened structure. Herein, the load level and the vertical convergence of the non-strengthened structure, when reaching the strengthening point, are denoted as P_0 and y_0, respectively. By analogy, the load level and the vertical convergence of the strengthened structure, when reaching the elastic limit and the bearing capacity limit, are denoted as P_e, y_e and P_u, y_u, respectively. The slope of the line ①–② in Figure 19 represents the stiffness of the strengthened structure, denoted as k_e. The stiffness before strengthening of the structure is denoted as k_0. The ductility is defined as $\Delta y = y_u - y_0$. The ratio of the strengthened structure to that of the non-strengthened structure is given as $R_P = P_u/P_0$, and the analogous ratio of the stiffness is given as $R_k = k_e/k_0$. The values of these indicators are listed in Table 5.

Table 5. Values of indicators in two different strengthening techniques. (Table view)

	SPPCS strengthening	EBSP strengthening
P_0 [kN]	452	418
y_0 [mm]	125	127
P_e [kN]	672	586
y_e [mm]	142	138
P_u [kN]	768	586
y_u [mm]	190	138
k_0 [kN / mm]	0.298	0.741
k_e [kN / mm]	12.854	15.506
Δy [mm]	65	11
R_P	1.70	1.40
R_k	43.16	20.93

In case of the EBSP strengthening technique, the area of the steel plate is $850 \times 20 mm^2$, whereas in case of the SPCCS strengthening technique, it is $1200 \times 10 mm^2$. Thus, the SPCCS strengthening technique results in a reduction of the area of the steel plate by 29%, but, at the same time, in an increase of the bearing capacity by 31%. As described in the Introduction, in the EBSP strengthening technique,

because of the high self-weight of the steel plate, hoisting machines are required, which reduces the construction efficiency. In the SPCCS strengthening technique, however, a hoisting machine is not required, because of the reduction of the area of the steel plate. This facilitates rapid construction. The ratio of the bearing capacity of the strengthened structure to the one of the non-strengthened structure increases by 21%. Although the structural stiffness decreases by 17%, the ratio of the stiffness of the strengthened structure to the one of the non-strengthened structure increases by 106%, and the ductility increases by 501%. Generally, the SPCCS strengthening technique results in a decrease of the area of the steel plate. At the same time, it leads to an increase of the strengthening benefits, as compared to the EBSP strengthening technique.

5. Conclusions

The following conclusions are drawn from the experimental investigation reported in this paper:

1. The new strengthening technique for segmental linings, reported in this paper, results in a significant increase of the bearing capacity, the structural stiffness, and the ductility. Moreover, the strengthening material is used effectively in the sense that the amount of steel required for the steel plate is reduced. This results in a reduction of the self-weight of the strengthening material and, thus, in an increase of the construction efficiency compared to the alternative strengthening technique.
2. Failure of the strengthened structure is characterized by a high degree of ductility. Four plastic hinges develop successively during the failure process. The load level corresponding to the development of the fourth plastic hinge is defined as the bearing capacity limit. It is worth mentioning that most of the plastic hinges occur at the segmental joints.
3. From a comparison with the EBSP strengthening technique, it is concluded that the SPCCS strengthening technique results in a higher degree of ductility of the structure. As for the strengthening benefits, the SPCCS technique allows for a decrease of the area of the steel plate. Moreover, it results in a significant increase of the strengthening benefits.
4. In the SPCCS strengthening technique, the bond established by a combination of studs, embedded steel bars, adhesive anchors, and steel-fiber reinforced concrete, has a high degree of strength and ductility. This ensures that the steel plate acts together with the original structure, resulting in full use of the material. There is little failure of bond between the steel plate and the concrete.

The experimental results obtained in this research provide the basis for further investigations. They serve as a reference for the application of the SPCCS strengthening technique. In the present research, because of the dimensions of the strengthening material layers, the inner space of the tunnel is decreased by 120 mm. In other applications, the available inner tunnel space should be checked. A reliable model will be used for parametric analysis, the results of which will provide guidelines for further work, recommending the application of the SPCCS strengthening technique.

Disclosure statement

No potential conflict of interest was reported by the author(s).

Funding

This research was financially supported by the National Natural Science Foundation of China (Grant No. 52078376, 52038008), the State Key Laboratory for Hazard Reduction in Civil Engineering, Tongji University (Grant No. SLDRCE19-B-39).

References

Blom, C. B. M. (2002). Design philosophy of concrete linings for tunnels in soft soils (PhD dissertation). Delft University of Technology, Delft, The Netherlands.

Chang, C. T., Sun, C. W., Duann, S. W., & Hwang, R. N. (2001). Response of a Taipei rapid transit system (TRTS) tunnel to adjacent excavation. *Tunnelling and Underground Space Technology*, *16*(3), 151–158.

Hua, J., Huang, L., Luo, Q., Chen, Z., Xu, Y., & Zhou, F. (2020). Prediction on the shrinkage of concrete under the restraints of steel plates and studs based on the capillary tension theory. *Construction and Building Materials*, *258*, 119499.

Jiang, Z., Liu, X., Schlappal, T., Zhang, J. L., Mang, H. A., & Pichler, B. (2020). Asymmetric serviceability limit states of symmetrically loaded segmental tunnel rings: hybrid analysis of real-scale tests. Tunnelling and Underground Space Technology (under review).

Kiriyama, K., Kakizaki, M., Takabayashi, T., Hirosawa, N., & Imafuku, K. (2005). Structure and construction examples of tunnel reinforcement method using thin steel panels. *Nippon Steel Technical Report*, *92*, 45–50.

Kozma, A., Odenbreit, C., Braun, M. V., Veljkovic, M., & Nijgh, M. P. (2019). Push-out tests on demountable shear connectors of steel-concrete composite structures. *Structures*, *21*, 45–54.

Li, X., Yan, Z., Wang, Z., & Zhu, H. (2015a). Experimental and analytical study on longitudinal joint opening of concrete segmental lining. *Tunnelling and Underground Space Technology*, *46*, 52–63.

Li, X., Yan, Z., Wang, Z., Zhu, H., & Wang, Z. (2015b). A progressive model to simulate the full mechanical behavior of concrete segmental lining longitudinal joints. *Engineering Structures*, *93*, 97–113.

Liu, X., Bai, Y., Yong, Y., & Mang, H. A. (2016). Experimental investigation of the ultimate bearing capacity of continuously jointed segmental tunnel linings. *Structure and Infrastructure Engineering*, *12*(10), 1364–1379.

Liu, X., Erkmen, R. E., & Bradford, M. A. (2012). Creep and shrinkage analysis of curved composite beams with partial interaction. *International Journal of Mechanical Sciences*, *58*(1), 57–68.

Liu, X., Jiang, Z., Yuan, Y., & Mang, H. A. (2018a). Experimental investigation of the ultimate bearing capacity of deformed segmental tunnel linings strengthened by epoxy-bonded steel plates. *Structure and Infrastructure Engineering*, *14*(6), 685–700.

Liu, X., Jiang, Z., Yuan, Y., & Mang, H. A. (2018b). Numerical investigation of the mechanical behavior of deformed segmental tunnel linings, strengthened by epoxy-bonded filament wound profiles. *Tunnelling and Underground Space Technology*, *78*, 231–244.

Liu, X., Jiang, Z., & Zhang, L. (2017). Experimental investigation of the ultimate bearing capacity of deformed segmental tunnel linings strengthened by epoxy-bonded filament wound profiles. *Structure and Infrastructure Engineering*, *13*(10), 1268–1283.

Liu, X., Zhang, C., Zhang, C., & Jiang, Z. (2016). Experimental study on the longitudinal joint in shield tunnel reinforced with FRP material. *Journal of Railway Science and Engineering*, *13*(2), 316–324.

Liu, X., Zhang, C., Zhang, C., & Yuan, Y. (2017). Ultimate load-carrying capacity of the longitudinal joints in segmental tunnel linings. *Structural Concrete*, *18*(5), 693–709.

Lu, L., Lu, X., & Fan, F. (2011). Full-ring experimental study of the lining structure of Shanghai Changjiang tunnel. *Journal of Civil Engineering and Architecture*, *5*(8), 732–739.

Nakamura, H., Kubota, T., Furukawa, M., & Nakao, T. (2003). Unified construction of running track tunnel and crossover tunnel for subway by rectangular shape double track cross-section shield machine. *Tunnelling and Underground Space Technology*, *18*(2-3), 253–262.

Narayanan, R. (Ed.). (1988). *Steel-concrete composite structures*. New York: CRC Press.

Nie, J., Wang, Y., & Cai, C. S. (2011). Experimental research on fatigue behavior of RC beams strengthened with steel plate-concrete composite technique. *Journal of Structural Engineering*, *137*(7), 772–781.

Schreyer, J., & Winselman, D. (2000). Suitability tests for the lining for the 4th Elbe Tunnel Tube - Results of large-scale tests. *Tunnel*, *1*, 33–44.

Sohel, K. M. A., Liew, J. R., Yan, J. B., Zhang, M. H., & Chia, K. S. (2012). Behavior of steel–concrete–steel sandwich structures with lightweight cement composite and novel shear connectors. *Composite Structures*, *94*(12), 3500–3509.

Wu, D., Gao, W., Feng, J., & Luo, K. (2016). Structural behaviour evolution of composite steel-concrete curved structure with uncertain creep and shrinkage effects. *Composites Part B: Engineering*, *86*, 261–272.

Yuan, Y., Jiang, X., & Liu, X. (2013). Predictive maintenance of shield tunnels. *Tunnelling and Underground Space Technology*, *38*, 69–86.

Zhang, J. L., Hellmich, C., Mang, H. A., Yuan, Y., & Pichler, B. (2018). Application of transfer relations to structural analysis of arch bridges. *Computer Assisted Methods in Engineering and Science*, *24*, 199–215.

Zhang, J. L., Liu, X., Ren, T. Y., Yuan, Y., & Mang, H. A. (2019). Structural behavior of reinforced concrete segments of tunnel linings strengthened by a steel-concrete composite. *Composites Part B: Engineering*, *178*, 107444–107441.

Zhang, J. L., Mang, H. A., Liu, X., Yuan, Y., & Pichler, B. (2019). On a nonlinear hybrid method for multiscale

analysis of a bearing capacity test on a real-scale segmental tunnel ring. *International Journal for Numerical and Analytical Methods in Geomechanics*, *43*(7), 1343–1372.

Zhang, J. L., Vida, C., Yuan, Y., Hellmich, C., Mang, H. A., & Pichler, B. (2017). A hybrid analysis method for displacement-monitored segmented circular tunnel rings. *Engineering Structures*, *148*, 839–856.

Zhao, H., Liu, X., Bao, Y., Yuan, Y., & Bai, Y. (2016). Simplified nonlinear simulation of shield tunnel lining reinforced by epoxy bonded steel plates. *Tunnelling and Underground Space Technology*, *51*, 362–371.